Journal of Nuclear and Radiochemical Sciences, Vol. 5, No.1, pp. R9-R17, 2004

Nuclear and Electronic Sputtering Induced by High Energy Heavy Ions

N. Imanishi* and S. Ninomiya

Department of Nuclear Engineering, Kyoto University, Sakyo, Kyoto 606-8501, Japan

Received: March 10, 2004; In Final Form: May 24, 2004

This review focuses on recent fruitful findings of dependence of sputtering phenomena on solid-state property and secondary particle species in the field of interaction of MeV-energy heavy ions with matter. Emission mechanism of singly charged ions from non-insulating targets is explained by the Sigmund-Thompson linear cascade model combined with increase of ionization probability by transient electronic excitation. However, emission mechanism of multiply charged ions differs from that of singly charged ions, and can be explained by a combined mechanism of simultaneous recoiling and ionization by the projectile and the Coulomb repulsion by a short-lived ionized track region. Large cluster ions are produced from non-metallic targets. Mostly clusters are emitted directly from solid surface. However, in the case of Al_2O_3, they are produced by coagulation of small molecules in a selvage region near the surface.

1. Introduction

When an energetic particle comes into a solid, collisions induce several processes such as recoil and sputtering of constituent atoms, defect formation, electron excitation and emission, and photon emission. The sputtering process, especially emission process of secondary ions, has been widely studied for various target materials under bombardment of heavy ions. Most of studies are, however, concerned with secondary ion mass spectrometry (SIMS) at nuclear-collision-dominant low energies.[1–7] In a MeV-energy range, an electronic-energy-loss process becomes dominant,[8] and the basic process of secondary ion emission is different from that in the low energy range because the electronic behavior strongly depends on the solid state property. How does the high-density electronic excitation energy deposited by a heavy ion transfer to the atomic motion? The problem was reviewed only for frozen gases and organic molecules.[9–16] The aim of this review is to show experimental results of yields and energies of secondary ions emitted from several tightly bound metallic, semiconductive, and insulating solid targets and to summarize the dynamic mechanism of secondary ion emission in the MeV-energy range by relating it to characteristic physical properties of the target materials.

2. Energy Deposition

An energetic ion incident on a solid collides with constituent atoms. Because of a large mass difference between the nucleus and the electron, the collision with the nucleus is called an elastic or a nuclear collision, where kinetic energy and momentum should be conserved during the collision. The collision with the electron is named as an inelastic or an electronic collision and results in excitation and ionization of constituent electrons in the atom. Thus, the ion passing through matter loses its kinetic energy by the electronic excitation and ionization and by the kinetic collision. The energy loss by the electron-related collision is called electronic or inelastic energy loss and the kinetic-collision induced energy loss is called nuclear or elastic energy loss. The former and the latter respectively work mainly at a high and a low velocity range. The term of stopping power is also used instead of the energy loss.

The most familiar stopping power formula is the Bethe-Bloch equation[17, 18] which is derived on the basis of the plane wave Born approximation applicable at a high velocity range. In a keV energy range, the ion velocity, especially that of a heavy ion, is very low and the nuclear collision could not be omitted. Lindhard, Scharff, and Schiott (LSS)[19] derived the universal electronic and nuclear stopping power formulae based on the Thomas-Fermi atomic model at the low velocity range. The Bethe-Bloch and the LSS formulae are underlying stopping power formulae in the high- and the low-energy range, respectively. However, obtained experimental values of stopping power depend so much on incident ion and energy, and target atom. Ziegler et al.[8] have developed a versatile program named SRIM covering stopping power, range, range straggling, damage distribution, sputtering yield, and so on and covering any incident ion-target atom combinations over an energy range between 1 keV and 2 GeV. In this review the nuclear and the electronic stopping powers are calculated with the SRIM code. Examples of the results are shown in Figure 1 for C, Si, and Ag projectiles passing through a Si target.

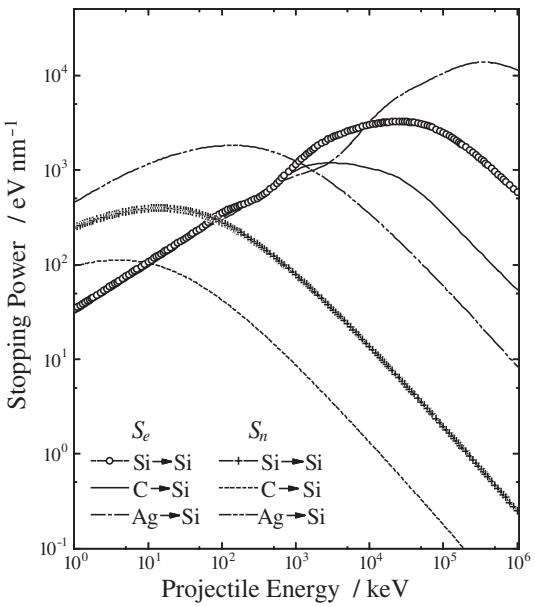

Figure 1. The SRIM (Reference 8) calculation of the nuclear and electronic stopping powers of a Si target for C, Si, and Ag projectiles.

*Corresponding author. E-mail: imanishi@nucleng.kyoto-u.ac.jp. FAX: +81-742-45-2356.

Published on Web 06/16/2004

3. Outline of Nuclear Sputtering –Low Energy Ion Bombardment–

On the basis of the binary-collision approximation (BCA) Sigmund proposed a linear collision cascade model, which has been successfully applied in a low energy-density collision.[20] When sputtering yield, Y, is defined as an average number of atoms removed from a solid surface per incident particle, the yield for backward sputtering at perpendicular incidence is given by

$$Y = \frac{0.042\alpha(M_2/M_1)S_n(E, Z_1, Z_2)}{NU_0}, \quad (1)$$

where S_n is a nuclear stopping power, Z_1 and Z_2 are, respectively, the atomic numbers of a projectile and a target atom, E is a projectile energy, N a density of the target material, U_0 an average surface-binding energy, and α is a function depending on the mass ratio between the target (M_2) and projectile (M_1) atoms.

Particles sputtered from a solid surface during particle bombardment are mostly neutral atoms emitted with a cosine like angular distribution and with a broad energy distribution that peaks at a few eV, about half the surface binding energy. Experimental data are often compared with the Sigmund-Thompson distribution[20–22] as described by

$$\frac{d^3Y}{dKd^2\Omega} \propto \frac{K}{(K+U_0)^{3-2m}}\cos\Theta, \quad (2)$$

where K and Θ are, respectively, a kinetic energy and a polar angle of the emitted particle with respect to the surface normal, Ω is a solid angle, and m an adjustable parameter close to 0.

Main parts of the sputtering phenomena can be understood by analytical linear cascade models and by associated computer simulation schemes of binary-collision approximation and Monte Carlo treatments, as far as an energy deposit to the target is small enough to be treated in the linear cascade regime and the contribution of the electronic excitation is small. In the case of high-energy deposition, various phenomena have been observed as spikes, large cluster emission, chemical effects, and so on. Therefore, the further understanding of these sputtering phenomena needs molecular dynamic treatments, because these phenomena contain many-body interactions, electron-phonon coupling, and internal excitation of a limited region.

Mass distributions of emitted neutral large clusters have been systematically measured by Wucher group using a post ionization method with a laser induced single ionization technique.[23, 24] The obtained cluster yields are very large and show a power law dependence n^δ on the cluster size n. The exponent δ depends on the total sputtering yield and wave length of ultraviolet.

In sputtering experiments on nonmetals measured yields are generally different from the expectations by the collisional theory. Here besides the energy transferred to target atoms by elastic collisions, the energy transferred to electrons producing electronic excitation and ionization also can contribute to atomic displacements. The sputtering mechanism for the nonmetals is material dependent and very complex.[25] Stampfli[26] proposed that a dense electronic excitation of electrons from valence band states of insulators or semiconductors to conduction band states induces an expansion of the bond lengths and results in sputtering. Delcorte et al. carried out a molecular dynamics simulation, which uses the adaptative intermolecular Brenner potential (AIREBO) including long-range van der Waals forces,[27] for organic solids bombarded by low energy Ar ions, and concluded that the atomic collision dissipates energy over the first few hundreds of femtoseconds, including bond-scissions in the molecular backbone and creating ultimately vibrational excitation and collective motion at the molecular scale.[28]

4. Sputtering Induced by High Energy Heavy Ions –Cooperation of Nuclear and Electronic Collisions–

4.1. Atomic Ion Emission

4.1.1. Yield. Figure 2 shows typical examples of light mass regions of time-of-flight (TOF) mass spectra for Al, Si, Al_2O_3, and SiO_2 targets bombarded by 3 MeV Si^{2+} ions. Singly and multiply charged atomic ions of the constituting elements are unambiguously identified in the spectra.[29] The corresponding spectra for GaP, GaAs, and GaSb targets are shown in Figure 3. Other than dominant species of $^{69,71}Ga^+$ ions, P ions are

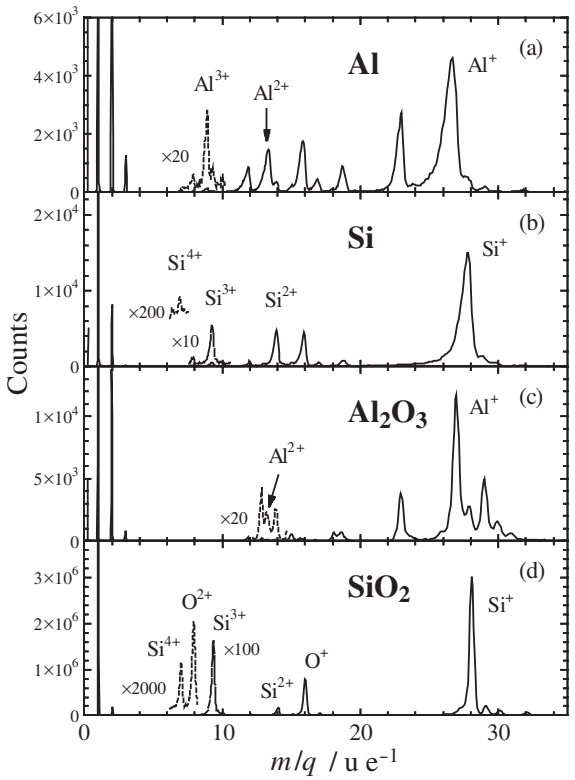

Figure 2. Light mass regions of TOF-mass spectra for Al, Si, Al_2O_3, and SiO_2 targets bombarded by 3 MeV Si^{2+} ions.

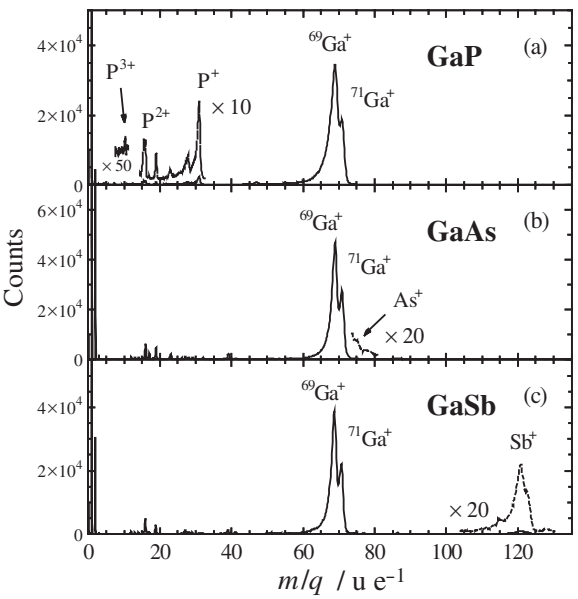

Figure 3. Light mass regions of TOF-mass spectra for GaP, GaAs, and GaSb targets bombarded by 3 MeV Si^{2+} ions.

unambiguously present as singly to triply charged positive ions but ^{75}As and $^{121,123}Sb$ ions are scantly observed.[30] The feature of very low yield of As ions was found for the low-energy sputtering of GaAs, too,[2] and it is caused by the high ionization potential of As atoms in addition to its heavy mass. Respective atomic ion yields are plotted in Figure 4 as a function of incident Si^{2+} ion energy. The yields of ions with $q=1$ except for the group V^{th} elements keep constant or slightly decrease with increasing incident energy, but those for the group V^{th} elements steeply increase with increasing energy.[30]

In order to understand the energy dependence of the yield, detailed data for Si and SiO_2 samples bombarded by C, Si, Ge, and Ag projectiles are shown in Figure 5, and the yields of Si^+ and Si^{4+} ions are plotted in Figure 6 as a function of S_n for the Si and SiO_2 targets.[31] In the Si^+-Si case, the experimental data are fitted well with a curve of $S_n^{0.78}$, and the fact implies that the Si^+ ions are still produced through the nuclear collision in the high-energy range. The same process can be applied for the emission of Al and Ga ions from the Al and GaV^{th} targets, respectively. However, the yields of the Si^+ ions from the SiO_2 target are higher than the corresponding yields from the Si target and don't correlate with the nuclear stopping power. The result of the SiO_2 target will be discussed later. In the case of Si^{4+}, as shown in Figure 6, the yield doesn't trace S_n. A promising mechanism of the emission of multiply charged ions should contain any direct ionization caused by the collisions of projectiles with target atoms. In fact multiply charged recoil ions are effectively produced in collision between energetic ions and rare-gas atoms, and the formation cross section can be given in the frame of the independent-electron model.[32–34] The model predicts that the multiply charged ions are produced by a transfer- and a pure-ionization process; in the former process ionization occurs following an exchange of electrons between the projectile and the atom, and in the latter process the projectile ionizes the atom without accompanying any electronic exchange. It is then plausible that the atoms on the surface are simultaneously ionized and recoiled by the same projectiles.

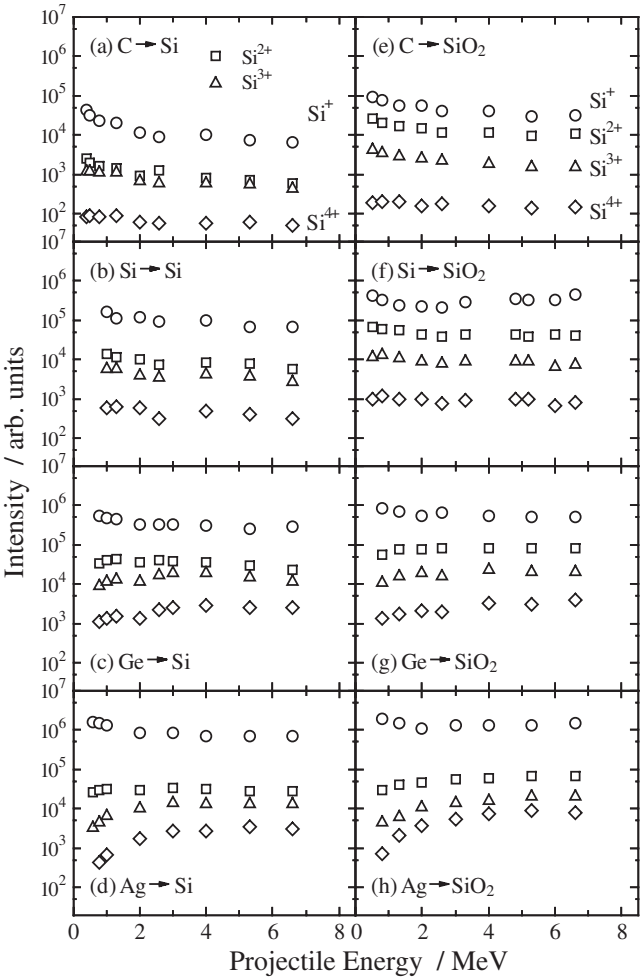

Figure 5. Energy dependence of the atomic ion yield for Si^+ (circles), Si^{2+} (rectangles), Si^{3+} (triangles), and Si^{4+} (diamonds) from Si and SiO_2 samples bombarded by C, Si, Ge, and Ag projectiles.

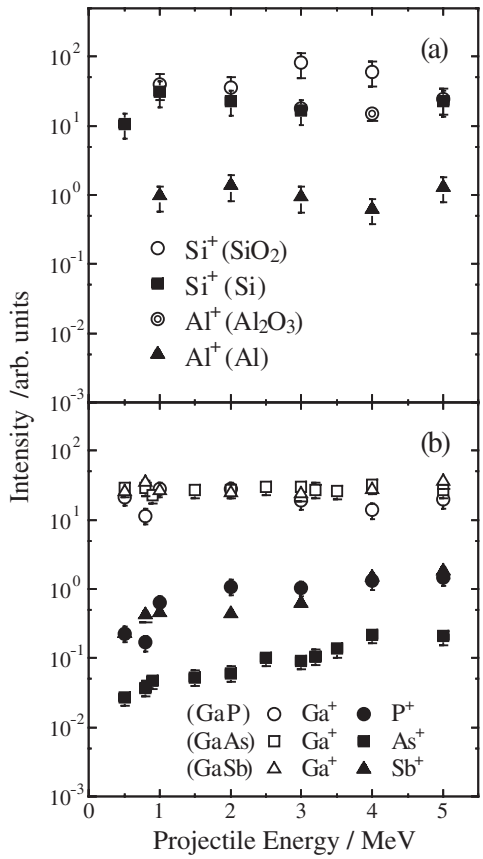

Figure 4. Singly charged atomic ion yields plotted as a function of Si projectile energy.

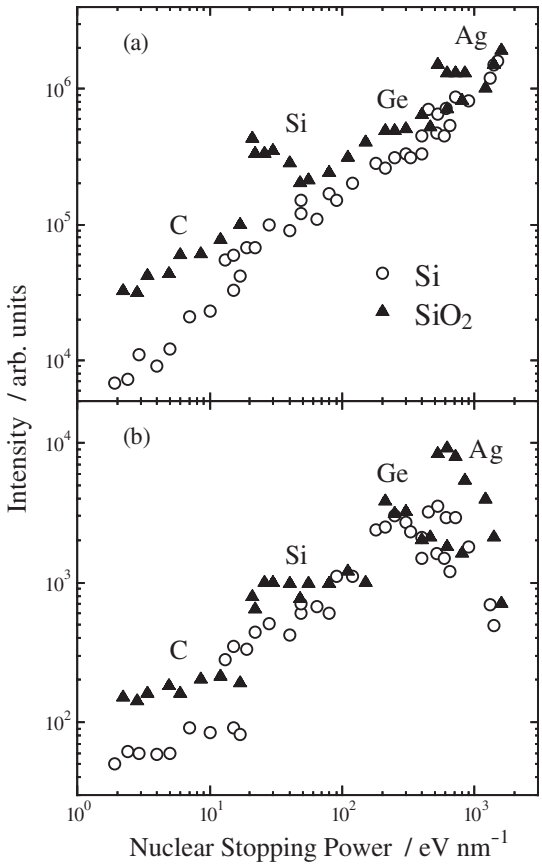

Figure 6. The yields of (a) Si^+ and (b) Si^{4+} ions plotted as a function of S_n for the Si and SiO_2 targets.

According to the independent-electron model,[32–34] the cross sections for multiple ionization of recoiled-atoms are given by the sum of cross sections for the pure and transfer ionization, and are expressed as

$$\sigma(q, q'; i) = \int \binom{n}{i} P_V^i (1-P_V)^{n-i}\, 2\pi b db, \tag{3}$$

where q and q' are the charges of projectiles before and after the collision, respectively, i is the charge of the recoiled ions, n the number of electrons in the outer shell, P_V the ionization probability of one of the outer-shell electrons, and b the impact parameter of collisions. For the transfer ionization P_V is assumed to be constant inside an impact parameter r_V and zero outside.[34] Then, the cross sections for those processes are expressed as follows:

$$\sigma(q, q'; i) = \binom{n}{i} P_V^i (1-P_V)^{n-i}\, r_V^2 \pi. \tag{4}$$

On the other hand for the pure ionization it is better to assume that the parameter P_V depends exponentially on the impact parameter,[34]

$$P_V(b) = P_V(0)\exp(-b/r_V), \tag{5}$$

where $P_V(0)$ represents the ionization probability of the outer-shell electrons at the impact parameter $b = 0$. The ionization cross sections calculated for the Si target (where $n = 4$) using the parameter values in Table 1 are plotted in Figure 7 along with the experimental data for the Si-Si system.[31] Those parameter values are derived from the results for a Ne^{q+} + Ne system at an energy of 1.05 MeV/u. The qualitative agreement supports the process caused by simultaneous occurrence of ionization and recoil induced by the projectiles.

TABLE 1: Values of the Parameters P_V and r_V (in nm) Used for (a) the Transfer Ionization and Those of $P_V(0)$ and r_V for (b) the Pure Ionization (Reference 31)

	q	q'	P_V	r_V
(a) transfer ionization	2	3	0.19	0.049
	2	4	0.28	0.036
	4	3	0.34	0.007
(b) pure ionization	2	2	0.35	0.033
	4	4	0.40	0.055

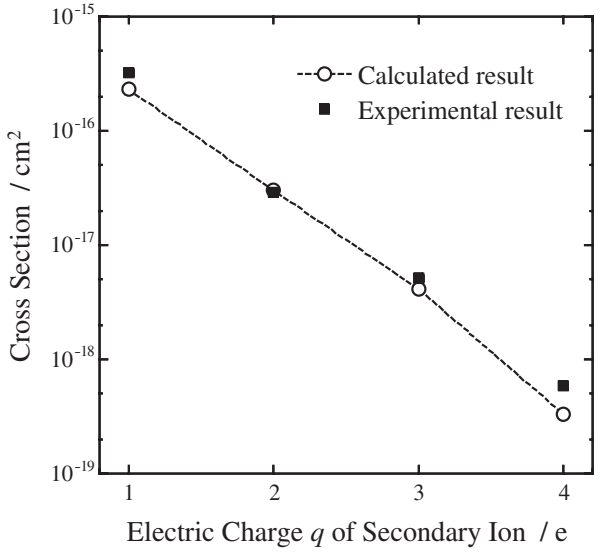

Figure 7. The ionization cross sections calculated (open circles) for the Si target (where $n = 4$) applying parameters derived from the results for a Ne^{q+} + Ne system at an energy of 1.05 MeV/u along with the experimental data (closed rectangles) for the Si-Si system. The line is drawn to guide the eye.

Another feature shown in Figure 4 is that the yields of the group Vth ions, whose ionization potentials are higher than the work functions of the samples, depend strongly on the incident energy (and the electronic stopping power). This characteristic dependence different from those of the other secondary ions can be accounted by the following process[30]: In the case of semiconductive and insulating materials, the fast projectile excites electrons from the valence band to the conduction band and the produced electrons excite further other electrons to the conduction band. As a result, lots of electron-hole pairs are produced along the path of the projectile, forming a very short-lived electronically high-excited spot. The holes increase the ionization probability compared to the static valence band by acting as accepters of electrons in the emitting atom. Šroubek has deduced the ionization probability P_e^+ as a function of effective electron temperature parameter T_{eff} characterizing the electronic excitation,

$$P_e^+ = \exp\left(-\frac{I-\varphi-\frac{e^2}{4v_\perp t_0}}{k_B T_{eff}}\right), \tag{6}$$

where φ and t_0 are respectively the work function and the relaxation time of the excited spot, I and $v_\perp$ are respectively the ionization potential and the normal velocity of the emitting atom, k_B is the Boltzmann constant and e is the electronic charge.[35, 36] The effective electron temperature parameter T_{eff} is connected with the electronic stopping power S_e. Then, in the framework of the above transient electronic excitation model, it is expected that yields of secondary ions with high ionization potentials depend exponentially on $1/S_e$. This expectation is confirmed by the clear exponential dependence shown in Figure 8. The transient electronic excitation can explain the following particulars of observed secondary ion yields which are beyond the scope of the ordinary surface ionization process. The high yield of Si^+ compared to that of Al^+, as shown in Figure 4, can be understood by the reason that the high-excited spot sustains longer in Si than in Al.[30] In spite of the comparable ionization potential of P and As, P^+ ions are more frequently produced than As ions.[30] The fact comes partly by the low electron mobility in GaP of 300 $cm^2V^{-1}s^{-1}$ that is 0.03 times as high as that for GaAs,[37] and the resultant high transient value of T_{eff} is expected. Thus, the increase of the yields of the secondary ions whose ionization potentials are much higher than the work functions of the samples is caused

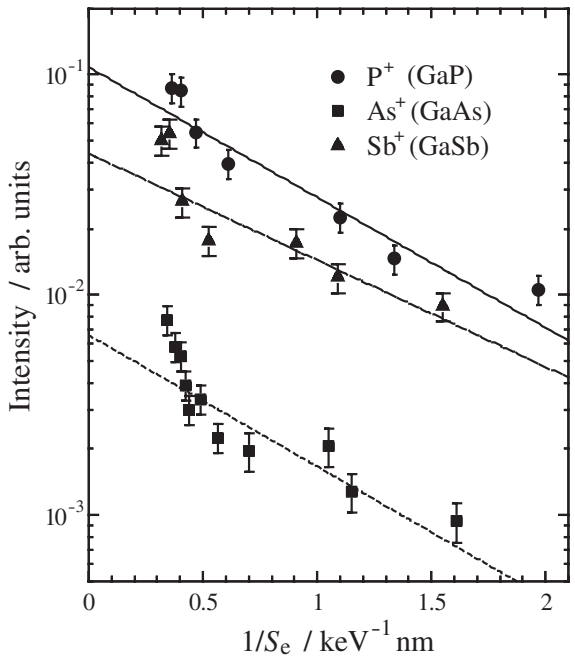

Figure 8. Secondary ion yields plotted as a function of $1/S_e$. The lines are drawn to guide the eye.

by the transient electronic excitation. That is, the electronic process plays an important role in the production of singly charged ions with high ionization potentials as well as multiply charged ions.

4.1.2. Energy Distribution. Particles sputtered from a solid surface have a broad energy distribution. An axial energy, which is defined as a kinetic energy along the surface normal, is usually measured and compared with theoretical results. The axial emission energy distributions for Al^{q+}, Si^{q+}, P^{q+} (*q*e: electric charge), and Ga^+ secondary ions are shown in Figure 9 for a 3 MeV Si^{2+}-ion bombardment, for example, and the result obtained for Ga^+ ions emitted from GaAs bombarded by 5.5 keV Ar^+ ions is also included.[2, 30, 38, 39] The distributions scarcely depend on the incident energy of Si ions and are strongly asymmetric extending to a high-energy side with a power law dependence on the emission energy. The Sigmund-Thompson calculation of the linear cascade model, which has been developed for sputtering in the nuclear-collision-dominant low incident energy region,[20–22] can reproduce the measured distributions using a reasonable surface potential energy of about 3 eV in the case of the singly charged ions even at the high energies, as far as noninsulating targets are concerned.[30, 38] The result agrees with the conclusion deduced from the yield measurement; that is, in the case of non-insulating targets, singly charged atomic ions are produced through the nuclear collision even in the high-energy range. In the case of insulating SiO_2 target, the energy distribution of Si^+ ions emitted from the target is symmetric and is narrower than the value expected from the Sigmund-Thompson distribution.[38] The result combined with the yield increase compared to the Si target leads to the conclusion that a large part of the secondary atomic ions are formed not by the linear collision cascade but mainly by a bond breaking through a repulsive energy level produced by the electronic process, as discussed earlier on laser-induced atomic desorption in some insulating materials such as alkali halides and SiO_2.[40, 41]

Regarding to the multiply charged ions,[30, 38] as shown in Figure 5, the observed yields are very high compared to data of the low-energy incidence. At a keV-energy region, a yield ratio of Si^{2+} to Si^{1+}, for example, is about 10^{-3} and it is explained by inner-shell excitations accompanied by Auger electron emission.[1] In this process, the emission energy distribution of multiply charged ions does not differ from that of singly charged ions. However, Figure 9 shows that the emission energy is higher than the value of the singly charged ions. The most probable and the mean energies of the axial emission energy distributions are overall proportional to the electric charge of the secondary ion, as shown in Figure 10 for the 3 MeV Si impact. These facts support the formation mechanism by the simultaneous process of ionization and kinetic recoil. The microscopic charging up in the track region stands for a very short period of about 10^{-15}–10^{-14} s. Then, the period is too short for a stationary atom to get a kinetic energy by the repul-

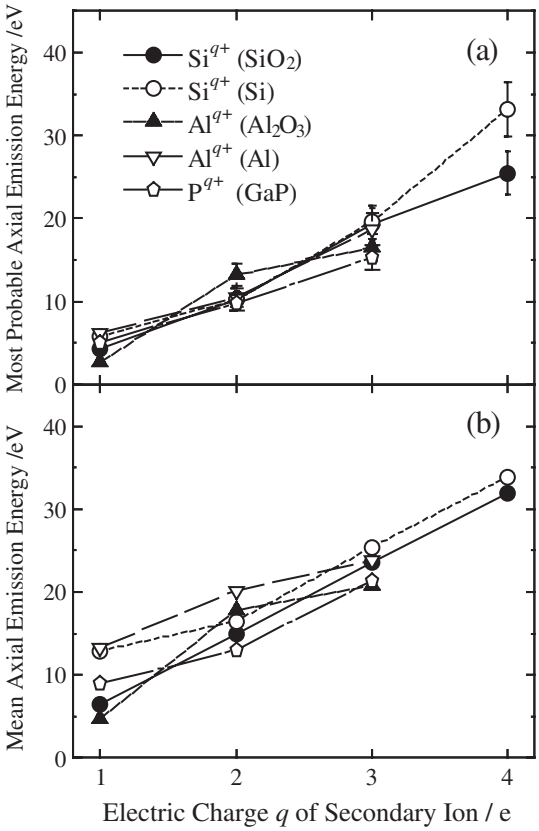

Figure 10. The most probable and the mean energies of the axial emission energy distributions for the 3 MeV Si^{2+} impact.

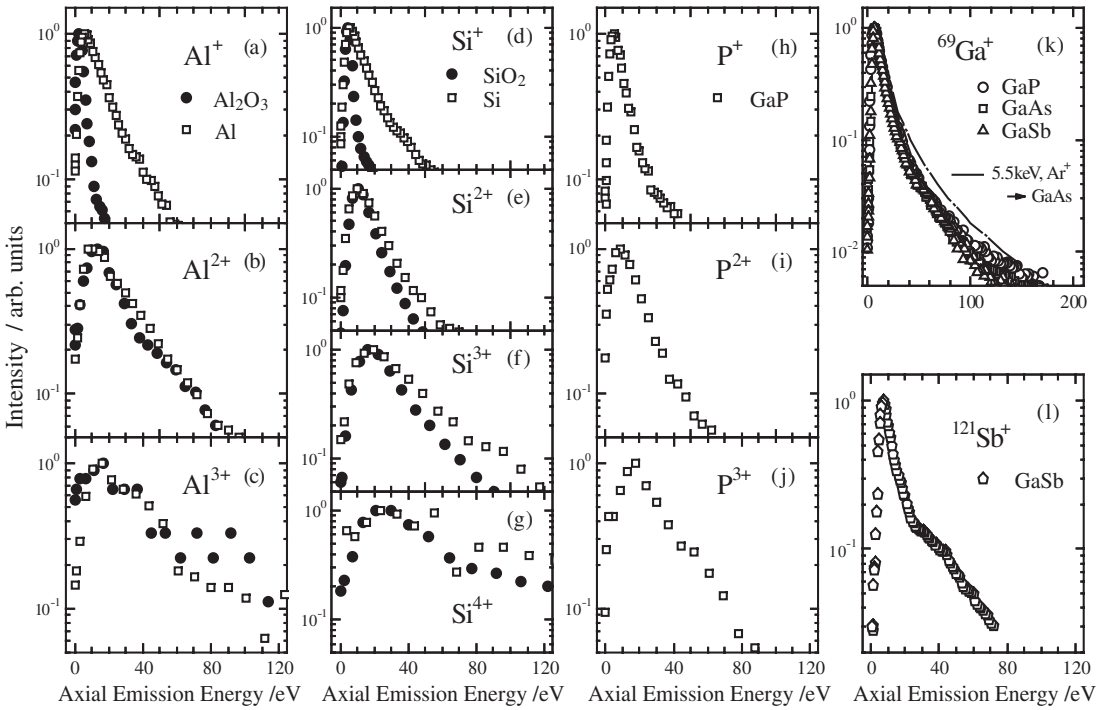

Figure 9. Axial emission energy distributions for Al^{q+}, Si^{q+}, P^{q+} (*q*e: electric charge), Ga^+, and Sb^+ secondary ions for the 3 MeV Si^{2+} impact along with the result obtained for Ga^+ ions emitted from GaAs bombarded by 5.5 keV Ar^+ ions.

sive Coulomb force enough to override the potential barrier. However, when a target atom on the surface is recoiled with a kinetic energy of a few eV to a direction of about 90° with respect to the incident beam axis, and is ionized at the same time, the atom is accelerated further to the backward direction by the repulsive Coulomb force from neighboring ionized target atoms in the track region and can get out the surface within 10^{-15}–10^{-14} s. The Coulomb repulsive energy is estimated to be about (10 to 15) × q eV on an average when the nearest lying atoms are assumed to be doubly ionized.[30] This simple mechanism initiated by the simultaneous recoiling and ionization is supported by the independence of the yield ratios on incident energy and target species.[31]

4.2. Cluster Ions

4.2.1. Yield. Figure 11 shows mass distributions of secondary ions emitted from Al, Al_2O_3, Si, SiO_2, GaP, GaAs, and GaSb under the bombardment of 3 MeV Si^{2+} ions. No cluster ion is emitted from the Al and Si targets. On the other hand, large cluster ions were observed for the Al_2O_3, and SiO_2 targets; $(Al_2O_3)_{p-1}AlO^+$, $(Al_2O_3)_{p-1}AlO_2^+$, $(Al_2O_3)_{p-1}Al_2O_2^+$, and $(Al_2O_3)_{p-1}Al_2O_3^+$ (p is a positive integer) from Al_2O_3, and $(SiO_2)_{p-1}Si^+$, $(SiO_2)_{p-1}SiO^+$, $(SiO_2)_{p-1}SiO_2^+$, and $(SiO_2)_{p-1}Si_2O^+$ from SiO_2.[42, 43] In the cases of the GaP and GaAs targets no large cluster ion was detected.[25] On the other hand, large cluster ions composed of Sb were found for the GaSb target.[25] The yields of the observed clusters emitted from SiO_2 are shown in Figure 12 as a function of the Si and Ag incident energy.[43] Figure 13 shows the case for the Si-GaSb system.[25]

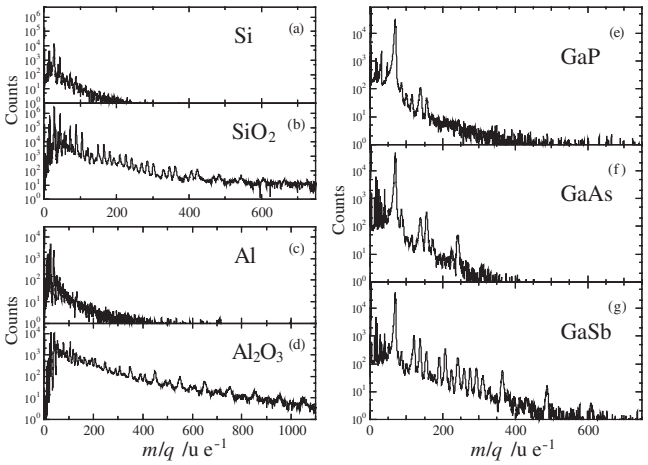

Figure 11. Mass distributions of secondary ions emitted from Al, Al_2O_3, Si, SiO_2, GaP, GaAs, and GaSb under the bombardment of 3 MeV Si ions.

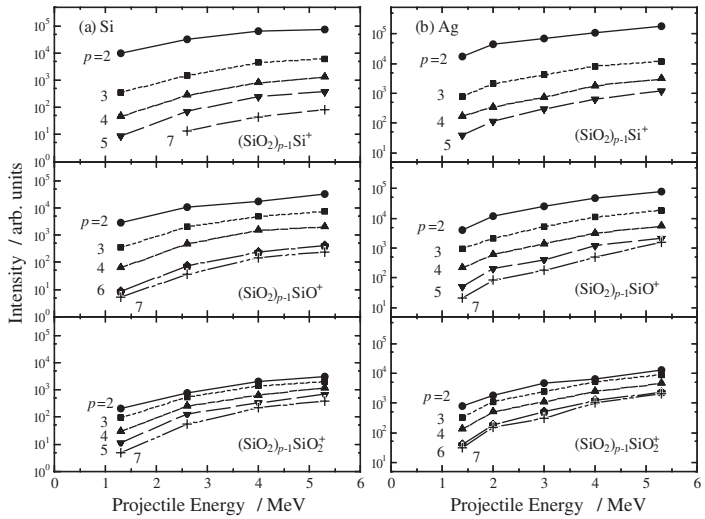

Figure 12. The yields of the observed clusters emitted from SiO_2 as a function of the (a) Si and (b) Ag incident energy.

We treat the mechanism of the sputtering from the SiO_2 sample.[43] The experimental result that the cluster yields steeply increase with increasing incident energy indicates that the electronic energy transfer governs the mechanism of cluster-ion formation even in the competing region of the electronic and nuclear energy depositions. Figures 14 and 15 show power law dependences of the cluster ion yields on the electronic stopping power and on the cluster size p, respectively.[43] From the results, it is obvious that the yields are represented well by a simple power function of $Y \propto p^A S_e^B$, where A and B are fitting parameters, A taking a negative value and B being positive. That is, the intensity of the cluster ions depends inversely on the size of the clusters and the intensity of the large cluster ions increases more steeply with increasing electronic stopping power than that of the small clusters. The unambiguous correlation indicates that the cluster ions are produced through the process initiated by the electronic-energy deposition. Mechanisms based on the electronic energy deposition have been proposed for the explanation of secondary-particle emission under high-energy ion bombardment.[10, 13, 14, 44] However, most of the models try to explain the total yield of the secondary particles and do not step into the explanation of the yields of individual components. Hedin et al.[12] proposed an ion-track model. In this model, it is assumed that secondary electrons produced by a projectile hit bonding electrons in a solid and a cluster with a size of p is emitted by multiple hits. The probability emitting the cluster depends both on the electronic stopping power and size. The larger cluster has the steeper increase with the stopping power. The prediction qualitatively explains the feature of the experimental dependence. That is, the cluster ions are not formed by the coagulation of SiO_2 molecules in a vacuum nor formed by decomposition of very large metastable clusters after sputtering, but are formed in the near-surface region due to the multiple breaking of bonds directly by the incident ions and indirectly by the shower of secondary electrons. For the Ag projectile 60% of the deposit energy, that is, 500 – 1000 eV/nm, is consumed in the excitation process of bonding electrons and sufficient to break a large number of covalent bonds (4.7 – 8.2 eV/bond) at the same time.[45]

On the other hand, the ion-track model cannot be applied to the semiconductive materials because of the fast recovery of

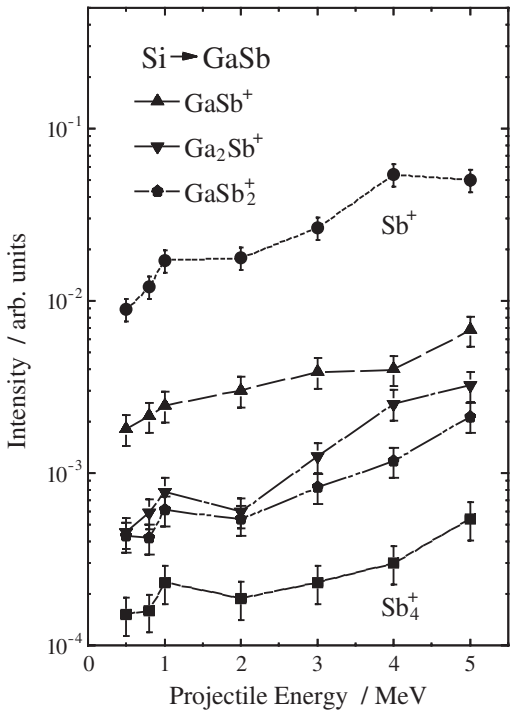

Figure 13. The yields of the observed clusters emitted from GaSb as a function of the Si incident energy.

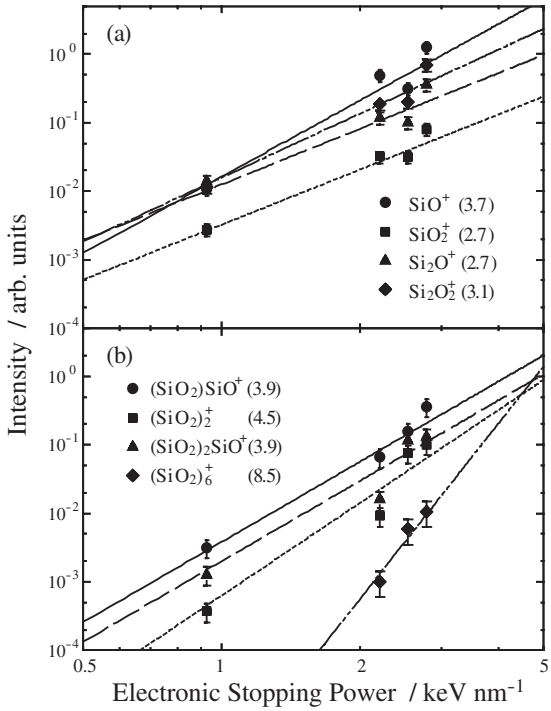

Figure 14. Power law dependences of the cluster ion yields on the electronic stopping power. The exponents of the power law function are shown in the parentheses. The lines are drawn to guide the eye.

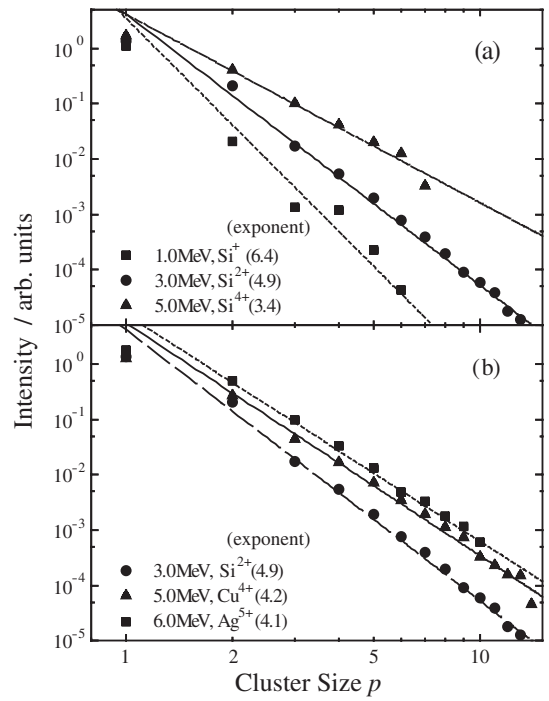

Figure 15. Power law dependences of the cluster ion yields on the cluster size p. The exponents of the power law function are shown in the parentheses. The lines are drawn to guide the eye.

the bond breaking. An experimental study of the sputtering phenomena of GaAs was done by Schenkel et al.[46, 47] using multiply charged slow ions. They plotted the total sputtering yield for GaAs as a function of potential energy, and found that the total yield is very low up to a value of the potential energy and then increases by two or three orders of magnitude beyond the value. Meanwhile, a theoretical work predicted that structural changes are induced in covalent solids when 10% of valence electrons are promoted from bonding states in the valence band to anti-bonding states in the conduction band.[48] Therefore, Schenkel et al.[46, 47] concluded that the steep increase of the sputtering yields is caused by the destabilization of atomic bonds resulted from high-density electronic

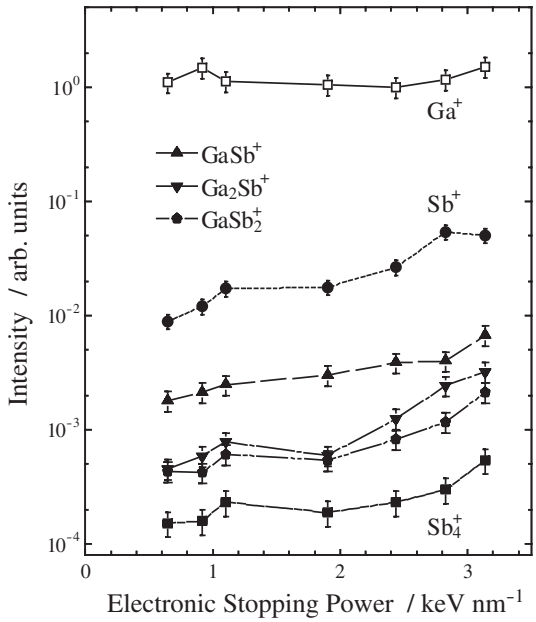

Figure 16. The yields of cluster ions from GaSb as a function of the electronic stopping power. The yield of Ga^+ is shown for comparison.

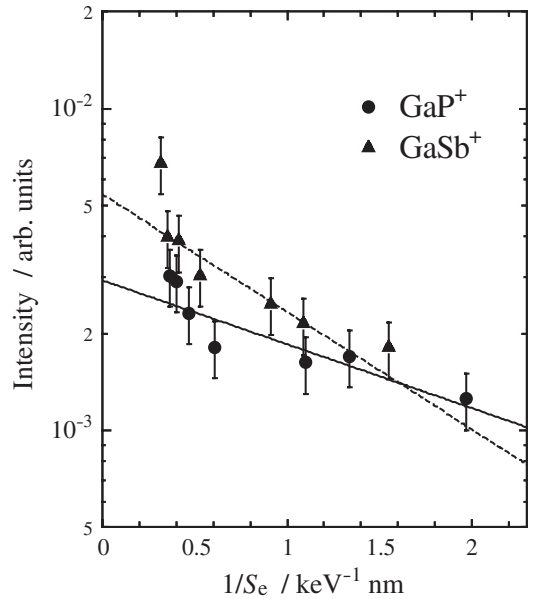

Figure 17. Secondary cluster ion yields plotted as a function of $1/S_e$ for the GaP and GaSb targets. The lines are drawn to guide the eye.

excitations. A critical laser fluence[49] to induce such a phase transition in GaAs is accepted to be 5 keV/nm^2 where a characteristic absorption depth[50] is 1 μm. Then a similar phase transition can happen for GaP, GaAs, and GaSb at the electronic stopping power of the MeV-energy region. The ionization potentials of a di-atomic cluster Ga_2 are low and they are easily ionized. Then, the yield dependence of Ga_2 ions on the incident energy is expected to represent the sputtering-yield dependence on the incident energy in the case of the GaVth targets.[51] As a result, the sums of the yields of neutral and ionized clusters containing Sb from GaSb should have a similar energy dependence.[51] However, as shown in Figure 16, the yields of the ionized clusters containing Sb increase with increase in the electronic stopping power; this behavior contrasts strongly with a scarce dependence of the Ga_2 ion yield on the electronic stopping power. The fact reflects the increase of ionization efficiency by the transient electronic excitation described above, as shown in Figure 17. Figure 18 shows the cluster size dependence of the secondary cluster ion yields for the GaSb target. The result shows the clear power-law dependence.

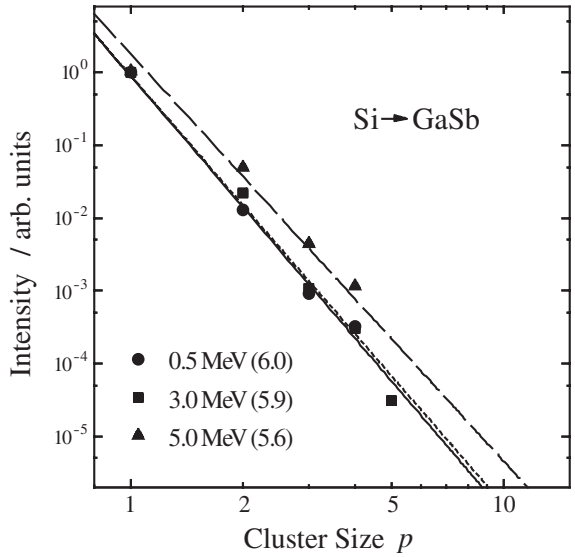

Figure 18. The cluster size dependence of the secondary cluster ion yields for the GaSb target bombarded by 0.5, 3, and 5 MeV Si ions. The exponents of the power law function are shown in the parentheses. The lines are drawn to guide the eye.

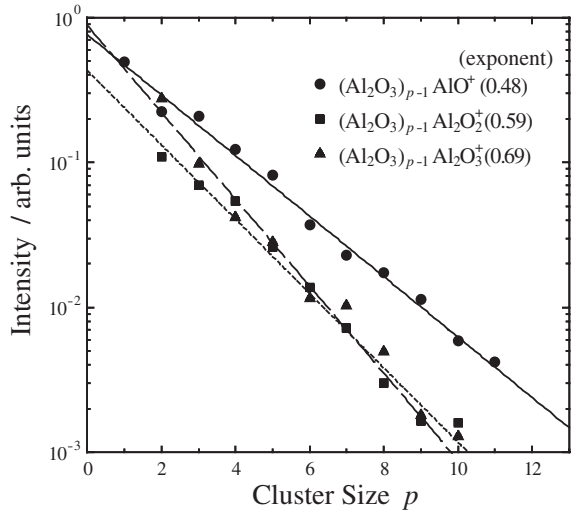

Figure 19. The cluster size dependence of the secondary cluster ion yield for Al_2O_3. The exponents of the power law function are shown in the parentheses. The lines are drawn to guide the eye.

So far quantitative explanation of the power-law dependence is still an open problem even in the nuclear-collision-dominant low energy sputtering.

Most experimental results of the yield dependence on size of cluster have shown power-law dependences irrespective of projectile energy. However, the result for Al_2O_3 shows exceptionally an exponential dependence as shown in Figure 19. The exponential dependence is expected in the process of coagulation of atoms and small molecules sputtered from the surface in a selvage region just outside the surface.[51]

4.2.2. Energy Distribution. As shown in Figure 20, axial emission energy distributions of oxide cluster ions from SiO_2 and Al_2O_3 are symmetric, and are very narrow compared to those of the atomic ions.[38] The peak energies are plotted in Figure 21 as a function of mass for the three series of the oxide clusters emitted from SiO_2 and Al_2O_3 in the 3-MeV Si incidences. In the case of SiO_2 the peak energy decreases very slowly with the size of clusters.[38] On the other hand, the energy of clusters from Al_2O_3 increases first with increasing size and then levels off.[51] The feature supports again that the clusters observed in Al_2O_3 are not directly emitted from the surface of the target but are probably produced indirectly by coagulation of molecules in the selvage region near the surface.

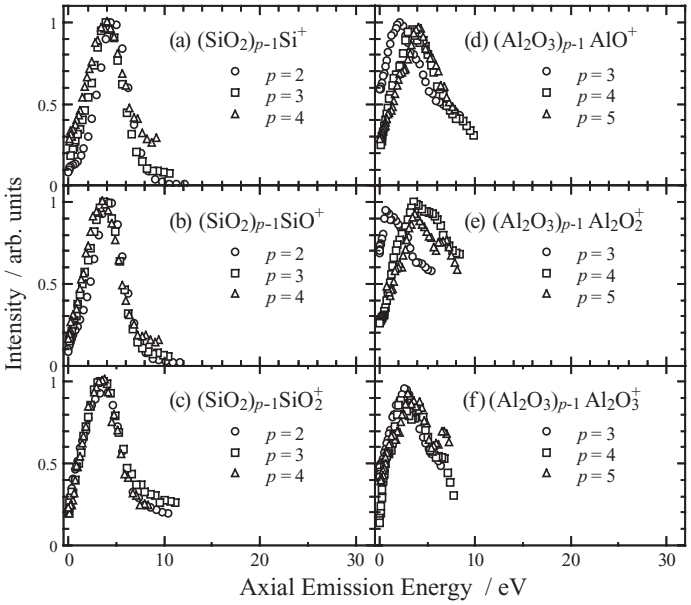

Figure 20. Axial emission energy distributions of oxide cluster ions from SiO_2 and Al_2O_3.

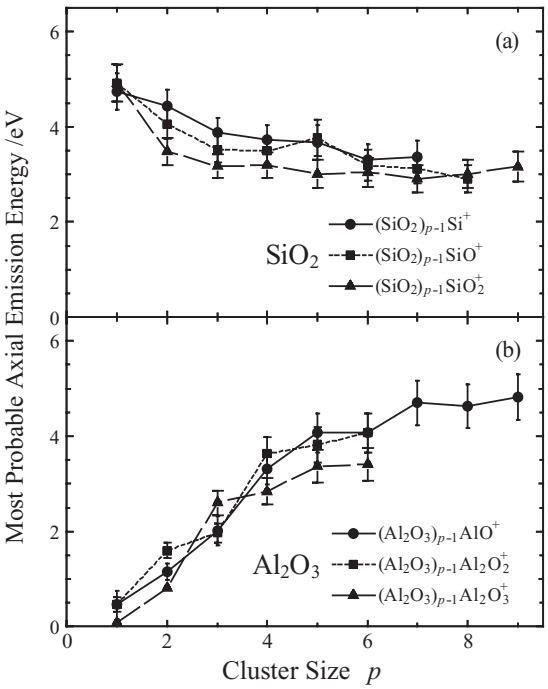

Figure 21. The peak energies plotted as a function of mass for the three series of the oxide clusters emitted from SiO_2 and Al_2O_3 in the 3 MeV Si^{2+} incidences.

5. Summary

The experimental results and the mechanism of secondary ion formation for the Al, Si, Al_2O_3, SiO_2, GaP, GaAs, and GaSb targets under MeV-energy heavy ion bombardment are presented. The secondary ion emission depends characteristically both on the secondary ion species and on the target species.

The yield and the emission energy distribution for the singly charged ions from the non-insulating targets are explained qualitatively by the Sigmund-Thompson linear cascade model combined with the increase of ionization probability by the transient electronic excitation.

However, the results for the multiply charged ions differ from those of the low-energy incidence in the high yield and the proportionality of the most probable and mean energies to the electric charge. The facts can be explained by the simple

combined mechanism of the simultaneous recoiling and ionization by the projectile and the Coulomb repulsion by the short-lived ionized track region.

Large cluster ions are produced from the Al_2O_3, SiO_2, and GaSb targets. The clusters from SiO_2 and GaSb are emitted directly from the surface. On the other hand, the clusters observed for Al_2O_3 are probably produced indirectly by coagulation of molecules in a selvage region near the surface.

References

(1) L. Yu Ming, in R. Behrisch, and K. Wittmaack (Eds.), *Sputtering by Particle Bombardment III*, Springer, Berlin-Heidelberg, 1991, p. 91, and references cited therein.
(2) W. M. Lau, Nucl. Instr. Meth. B **16**, 41 (1986).
(3) W. O. Hofer and H. Gnaser, Nucl. Instr. Meth. B **18**, 605 (1987).
(4) D. van Leyen, B. Hagenhoff, E. Niehuis, and A. Benninghoven, J. Vac. Sci. Tech. A **7**, 1790 (1989).
(5) R. Blumenthal, K. P. Caffey, E. Furman, B. J. Garrison, and N. Winograd, Phys. Rev. B **44**, 44 (1991).
(6) M. A. Karolewski and R. G. Cavell, Surf. Sci. **480**, 47 (2001).
(7) S. F. Belykh, I. A. Wojciechowski, V. V. Palitsin, A. V. Zinoviev, A. Adriaens, and F. Adams, Surf. Sci. **488**, 141 (2001).
(8) J. F. Ziegler, J. P. Biersack, and U. Littmark, *The Stopping and Range of Ions in Solids*, Pergamon Press, New York, 1985.
(9) B. U. R. Sundqvist, in R. Behrisch and K. Wittmaack (Eds.), *Sputtering by Particle Bombardment III*, Springer, Berlin-Heidelberg, 1991, p.257, and references cited therein.
(10) R. E. Johnson, Int. J. Mass Spectrum Ion Process **78**, 357 (1978).
(11) R. E. Johnson and W. L. Brown, Nucl. Instr. Meth. **209/210**, 469 (1983).
(12) A. Hedin, P. Håkansson, B. U. R. Sundqvist, and R. E. Johnson, Phys. Rev. B **31**, 1780 (1985).
(13) I. S. Bitensky and E. S. Parilis, Nucl. Instr. Meth. B **21**, 26 (1987).
(14) D. Fenyö, B. U. R. Sundqvist, B. R. Karlsson, and R. E. Johnson, Phys. Rev. B **42**, 1895 (1990).
(15) R. M. Papaléo, G. Brinkmalm, D. Fenyö, J. Eriksson, H. -F. Kammer, P. Demirev, P. Håkansson, and B. U. R. Sundqvist, Nucl. Instr. Meth. B **91**, 667 (1994).
(16) K. Wien, Ch. Koch, and Nguyen van Tan, Nucl. Instr. Meth. B **100**, 322 (1995).
(17) H. Bethe, Ann. Phys. **5**, 325 (1930).
(18) F. Bloch, Z. Phys. **81**, 363 (1933).
(19) J. Lindhard, M. Scharff, and H. E. Schiott, Mat. Fys. Medd. Dan Vid. Selsk. **33**, (no. 14) 3 (1963).
(20) P. Sigmund, Phys. Rev. **184**, 383 (1969).
(21) P. Sigmund, in R. Behrisch (Ed.), *Sputtering by Particle Bombardment I*, Springer, Berlin-Heidelberg, 1981, p. 9.
(22) M. W. Thompson, Philos. Mag. **18**, 377 (1968).
(23) A. Wucher and M. Wahl, Nucl. Instr. Meth. B **115**, 581 (1996).
(24) C. Staudt and A. Wucher, Phys. Rev. B **66**, 075419 (2002).
(25) S. Ninomiya, S. Gomi, C. Imada, M. Nagai, M. Imai, and N. Imanishi, Nucl. Instr. Meth. B **209**, 233 (2003).
(26) P. Stampfli, Nucl. Instr. Meth. B **107**, 138 (1996).
(27) S. J. Stuart, A. B. Tutein, and J. A. Harrison, J. Chem. Phys. **112**, 6472 (2000).
(28) A. Delcorte, B. Arezki, P. Bertrand, and B. J. Garrison, Nucl. Instr. Meth. B **193**, 768 (2002).
(29) S. Ninomiya, S. Gomi, J. Xue, M. Imai, and N. Imanishi, *Proc. 16th Int. Conf. on Application of Accelerators in Research and Industry*, (AIP Press, New York, 2001) p. 543.
(30) S. Ninomiya, N. Imanishi, J. Xue, S. Gomi, and M. Imai, Nucl. Instr. Meth. B **193**, 745 (2002).
(31) S. Kyoh, K. Takakuwa, M. Sakura, M. Umezawa, A. Itoh, and N. Imanishi, Phys. Rev. A **51**, 554 (1995).
(32) R. E. Olson, J. Phys. B **12**, 1843 (1979).
(33) J. Ullrich, K. Bethge, S. Kelbch, W. Schadt, H. Schmidt-Böking, and K. E. Stiebing, J. Phys. B **19**, 437 (1986).
(34) H. Tawara, T. Tonuma, H. Kumagai, and T. Matsuo, Phys. Rev. A **41**, 116 (1990).
(35) Z. Šroubek, Phys. Rev. B **25**, 6046 (1982).
(36) Z. Šroubek, Nucl. Instr. Meth. **194**, 533 (1982).
(37) D. R. Lide (editor-in-chief), *CRC Handbook of Chemistry and Physics 81*. CRC Press, Boca Ralon, Florida, 2000-2001, pp. 12-105.
(38) N. Imanishi, H. Ohta, S. Ninomiya, and A. Itoh, Nucl. Instr. Meth. B **164-165**, 803 (2000).
(39) N. Imanishi, A. Shimizu, H. Ohta, and A. Itoh, *Proc. 15th Int. Conf. on Application of Accelerators in Research and Industry*, (AIP Press, New York, 1999) p. 396.
(40) M. Sporn, G. Libiseller, T. Neidhart, M. Schmid, F. Aumayr, H. P. Winter, and P. Varga, Phys. Rev. Lett. **79**, 5280 (1997).
(41) N. Itoh, Nucl. Instr. Meth. B **122**, 405 (1997).
(42) N. Imanishi, S. Kyoh, K. Takakuwa, M. Umezawa, Y. Akahane, M. Imai, and A. Itoh, *Proc. 14th Int. Conf. on Application of Accelerators in Research and Industry*, (AIP Press, New York, 1997) p. 507.
(43) N. Imanishi, S. Kyoh, A. Shimizu, M. Imai, and A. Itoh, Nucl. Instr. Meth. B **135**, 424 (1998).
(44) R. E. Johnson and W. L. Brown, Nucl. Instr. Meth. **209/210**, 469 (1983).
(45) J. B. Malherbe, S. Hofmann, and J. M. Sanz, Appl. Surf. Sci. **27**, 355 (1986).
(46) T. Schenkel, A. V. Hamza, A. V. Barnes D. H. Schneider, J. C. Banks, and B. L. Doyle, Phys. Rev. Lett. **81**, 2590 (1998).
(47) T. Schenkel, A. V. Hamza, A. V. Barnes, and D. H. Schneider, Prog. Surf. Sci. **61**, 23 (1999).
(48) P. Stampfli and K. H. Bennemann, Phys. Rev. B **49**, 7299 (1994).
(49) L. Huang, J. P. Callan, E. N. Glezer, and E. Mazur, Phys. Rev. Lett. **80**, 185 (1998).
(50) R. F. W. Herrmann, J. Gerlach, and E. E. B. Campbell, Appl. Phys. A **66**, 35 (1998).
(51) S. Ninomiya and N. Imanishi, Vacuum **73**, 79 (2004).